Wave model of the cat tympanic membrane

Pierre Parent[a)]
Mimosa Acoustics, Inc., 129, avenue du Général Leclerc 75014 Paris, France

Jont B. Allen
University of Illinois at Urbana-Champaign, Dept. of Electrical and Computer Engineering, Beckman Institute, Room 2061, 405 North Mathews, Urbana, Illinois 61801

(Received 22 August 2006; revised 20 April 2007; accepted 6 May 2007)

In order to better understand signal propagation in the ear, a time-domain model of the tympanic membrane (TM) and of the ossicular chain (OC) is derived for the cat. Ossicles are represented by a two-port network and the TM is discretized into a series of transmission lines, each one characterized by its own delay and reflection coefficient. Volume velocity samples are distributed along the ear canal, the eardrum, and the middle ear, and are updated periodically to simulate wave propagation. The interest of the study resides in its time-domain implementation—while most previous related works remain in the frequency domain—which provides not only a direct observation of the propagating wave at each location, but also insight about how the wave behaves at the ear canal/TM interface. The model is designed to match a typical impedance behavior and is compared to previously published measurements of the middle ear (the canal, the TM, the ossicles and the annular ligament). The model matches the experimental data up to 15 kHz. © *2007 Acoustical Society of America.* [DOI: 10.1121/1.2747156]

PACS number(s): 43.64.Bt, 43.64.Ha, 43.64.Kc [WPS] Pages: 918–931

I. INTRODUCTION

Understanding sound propagation in the ear is critical to our understanding of both the middle ear and the cochlea, and can have a significant impact on the diagnosis of hearing loss. Various diagnosis methods have been derived to isolate the different factors playing a role in the ear's response, both in the middle ear, such as otitis media with effusion (Allen *et al.*, 2005), and in the cochlea, such as damaged outer hair cells (Allen, 2001, 2003). Such models of middle ear and cochlear wave propagation may be roughly classified into two broad categories: distributed and lumped circuit models.

Lumped-parameter circuit representations are usually implemented in the frequency domain using electrical circuit analogies, including the first quantitative model of the cochlea (Wegel and Lane, 1924). In such models, elements of fluid or tissue are represented by inductors representing the element mass, and capacitors representing the stiffness. The analogy with the well-known electrical circuit theory makes this method quite intuitive to use. A key work in the field is the model of the middle ear by Zwislocki (1957,1962), which is based on impedance measurements performed on patients with normal and pathological ears. Due to the tympanic membrane's (TM's) complex geometry and nonrigid construction, and due to its distributed nature, this and other lumped-parameter models are not accurate above a few kHz (Puria and Allen, 1998). Furthermore, modeling details of cochlear and middle ear structures using lumped-parameter methods may require Herculean efforts. For example, modeling a delay in the TM would require a cascade of inductors and shunt capacitors; a second example is the two-piston TM model of Shaw (1977). On the other hand, in their favor, such works have been intuitive and promising starting points for many other models (Shaw and Stinson, 1981; Lynch *et al.*, 1982; Goode and Killion, 1987; Rosowski *et al.*, 1990; Puria and Allen, 1998).

Distributed models may be used when a precise physical model of the ear anatomy and geometry is required. Typically, those models would rely on a finite element analysis or an asymptotic approach, and make sense when it comes to studying complex anatomical structures, such as the eardrum (Funnel and Laszlo, 1978; Rabbitt and Holmes, 1986; Funnel *et al.*, 1987; Fay, 2001; Fay *et al.*, 2002). A clear strength of these models is that they can account for complex mechanical and physical constraints by accurate (but complex) representations of the eardrum behavior. Their main drawbacks reside in the complexity to generate the mesh representing the three-dimensional (3D) structure to be analyzed, their computational time, and that they, like the lumped models, are usually (but not necessarily) implemented in the frequency domain.

Shaw's early representation of the TM as a double-piston source (Shaw, 1977; Shaw and Stinson, 1981) enabled his model to produce a higher-modes response, improving its utility up to 6 kHz. Even better results could be obtained with more sophisticated models, but the number of parameters required to be accurate over an extensive range of frequencies may be unacceptable. All of these models ignore the simple physical source of higher order modes, namely delay. An alternative approach was suggested by Puria and Allen (1998), who represented the TM by a simple distributed transmission line to account for an observed delay, which they estimated from measurements. Using a parameter optimization algorithm, they found excellent agreement with cat impedance data from Allen (1986), over the entire fre-

[a)]Author to whom correspondence should be addressed. Electronic mail: pierre@mimosaacoustics.com

quency range, up to 30 kHz. A major weakness of this TM model is the lack of any impedance transformation, as required by an actual TM. The impedance transformation ratio between the ear canal and the middle ear is known to be around 30 (Bekesy and Rosenblith, 1951; Zwislocki, 1957). In fact, Puria and Allen (1998, page 3475) suggest a more subtle distributed model of the TM, formed by discretizing it into a set of concentric annuli of different impedances, ranging from the canal impedance at the membrane periphery, to the malleus impedance at its center, with the change in impedance along the TM radius being mainly due to its increasing stiffness. In the model presented here, these several ideas are implemented, using a time-domain reflectance model of the middle ear.

The interest of the present study resides in two main points. First, it aims at a full development of the conceptual TM model from Puria and Allen (1998), using a spatially dependent description of the impedance. Second, it uses a time-domain implementation. When a system is described by a lumped-parameter model, it is usually quite easy to derive its frequency response and inverse-Fourier transform it as a convolution in the time domain.

Distributed systems—such as the TM—are infinite order and require a high order approximation to be dealt with properly. A time-domain description only requires interactions of neighboring elements at each observation point and is therefore a computationally sparse representation since only nearest neighbor elements are involved with each time step update. Furthermore, nonlinear systems need to be studied in the time domain; in fact, they usually have to be described by a series of differential equations which need to be solved to represent the system's current state. Conversion from the frequency domain to such a family of equations can be difficult, especially when the order of the differential equations changes (e.g., at a horn's cutoff frequency). A direct time-domain approach is ideal in such cases (Parent, 2005; Parent and Allen, 2006) and has been used to model nonlinear phenomena such as those occurring in the cochlea (Sen and Allen, 2006). Finally, previous works (Allen, 1986; Puria and Allen, 1998) have concluded that the canal and the TM have frequency-independent delays, not always nicely represented by a cascade of mass and stiffness elements. Our approach is to implement this delay in the time domain using transmission lines.

This study is largely about the TM and its dynamics and response, as a variable impedance delay line and impedance matching device. The model is introduced and its results are compared to a range of experimental data. Since impedance is known to be a reliable measurement of the middle ear status (Allen *et al.*, 2005), the model parameters are adjusted to fit experimental impedance-related data from Allen (1986). Finally, the model's behavior is compared to ossicles displacements measurements by Guinan and Peake (1967).

II. BASIC ASSUMPTIONS

This section reviews our underlying assumptions regarding acoustics and transmission lines, and provides our notation.

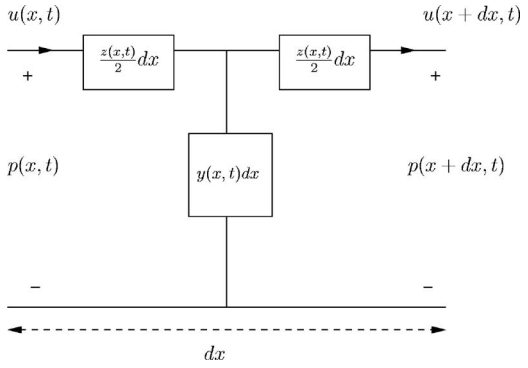

FIG. 1. Circuit representation for an element of transmission line. The series impedance is noted $z(x,t)$ and the shunt admittance is noted $y(x,t)$, in terms of their per unit length distributions (i.e., an impedance will be of the form $z(x,t)dx$).

Most transmission line elements can be approximated by the circuit in Fig. 1 (Brillouin, 1953; Beranek, 1954; Kinsler *et al.*, 2000). In the limit of small dx, this circuit represents a distributed medium. This one-dimensional approach to the middle ear is widely adopted (Rabbitt and Holmes, 1988; Stinson and Khanna, 1994). The pressure is denoted $p(x,t)$, and the volume velocity $u(x,t)$, both variables depending on their position along the propagation axis and on time. Let us define the Laplace variable, $s=i\omega$, where ω is the angular frequency. In the frequency domain, state variables are denoted $P(x,s)$ and $U(x,s)$ and, assuming a one-dimensional (1D) approximation, they are related by the impedance $z(x,t)\leftrightarrow Z(x,s)$ and admittance $y(x,t)\leftrightarrow Y(x,s)$ (Brillouin, 1953):

$$\frac{\partial}{\partial x}\begin{bmatrix} P(x,s) \\ U(x,s) \end{bmatrix} = -\begin{bmatrix} 0 & Z(x,s) \\ Y(x,s) & 0 \end{bmatrix}\begin{bmatrix} P(x,s) \\ U(x,s) \end{bmatrix}. \tag{1}$$

Assuming that no dispersion occurs, that the propagation is plane and lossless, and that impedances are constant along the small length dx, Eq. (1) leads to the classical d'Alembert solution in the time domain (Kinsler *et al.*, 2000):

$$p(x,t) = e^{st}(\mathbf{A}e^{-\gamma x} + \mathbf{B}e^{\gamma x}), \tag{2}$$

$$u(x,t) = e^{st}(\mathbf{C}e^{-\gamma x} + \mathbf{D}e^{\gamma x}), \tag{3}$$

where **A**, **B**, **C**, and **D** are four complex constants determined by the boundary conditions of the propagation. The complex wave *propagation factor* $\gamma(x,s)$ is defined via the impedance and admittance and given in the frequency domain by

$$\gamma(x,s) = \sqrt{Z(x,s)Y(x,s)}. \tag{4}$$

The pressure and velocity can then be decomposed into a positive (factor $e^{-\gamma x}$), and a retrograde component (factor $e^{\gamma x}$), indicated by superscripts ±.

Based on theoretical arguments (Stinson and Khanna, 1994; Lynch, 1981, pp. 146–148), Puria and Allen (1998) have underlined that the vibration propagation in the ear can be assumed to be plane below 25–30 kHz. In this case, p and u components are related by the medium *characteristic impedance*, $z_0(t)$:

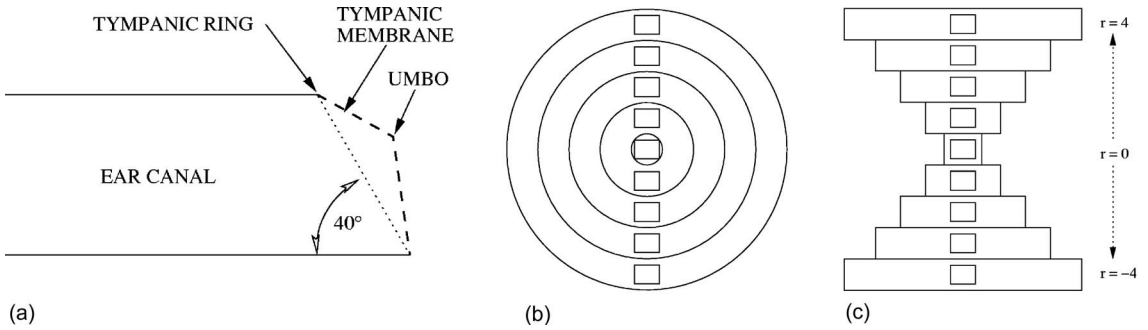

FIG. 2. Discretized tympanic membrane model for $N=5$. (a) Position of the TM in the ear canal. (b) The decomposition in annuli, respecting the circular geometry of the membrane. (c) The one-dimensional model that we actually use, derived from the previous one by applying mass conservation, indicated by the different widths of the stripes. The number of samples on TM is $2N-1$, i.e., nine in this example.

$$p^{\pm}(x,t) = z_0(t) \star u^{\pm}(x,t), \tag{5}$$

where $\star$ represents convolution. After some algebra $z_0(t) \leftrightarrow Z_0(s)$ can be expressed in terms of the circuit element impedances in the frequency domain

$$Z_0(s) = \frac{Z(s)}{\gamma(s)} = \sqrt{\frac{Z(s)}{Y(s)}}. \tag{6}$$

In nondispersive fluids, frequency dependencies in $Z(s) = sM$ and $Y(s) = sC$ cancel out so that $Z_0 = \sqrt{M/C}$ is independent of frequency. If the duct is presumed to be uniform, then Eq. (6) is the expression of the transmission line's characteristic impedance. The solution of the D'Alembert equation leads to the signal representation used in the model: two sets of transmission lines, one representing the forward-going wave and one representing the backward-going wave; both lines actually model the sound wave volume velocity. The use of this approach was first suggested by Kelly and Lochbaum (1963) and is a well-known method in vocal tract (speech) simulations.

In this work the "Kelly-Lochbaum" model is first applied to the ear canal. Since the canal is not perfectly straight, some minor reflections may occur during propagation (Stinson *et al.*, 1982; Stinson and Khanna, 1989; Stinson, 1990; Stinson and Khanna, 1994; Stinson and Daigle, 2005), but shall be ignored. In addition, in an intact ear, the canal opens at the pinna which has previously been modeled by a horn radiation impedance (Rosowski *et al.*, 1988), which for the human pinna has a cutoff that is presently undetermined. However, our study uses the same conditions as the measurements by Allen (1986), i.e., with the stimulus launched very close to the TM. It is therefore reasonable to approximate the remaining part of the canal by a lossless straight tube. Canal samples are then simply distributed along its length, Δx_{ec} apart, where Δx_{ec} is defined by

$$\Delta x_{ec} = \frac{\mathcal{C}_{ec}}{f_s}, \tag{7}$$

where the wave speed in the medium is $\mathcal{C}_{ec}$ and the sampling frequency f_s takes into account spatial sampling constraints of the ossicular chain (OC). The canal length is approximated by the closest multiple of Δx_{ec}, which for our choice of parameters (discussed below) represents a relative error of about 3%.

III. METHODS

This work uses two modeling approaches. The TM, as well as the ear canal, is represented by a distributed model which takes its space-varying properties into account. It is then attached into a classic lumped-parameter model of the OC (Zwislocki, 1962; Puria and Allen, 1998), as is explained in the following sections.

A. Tympanic membrane

The model of the TM is the gist of this study. This section describes basic anatomical aspects of this organ, then explains how it is modeled and interfaced with the model of the ear canal.

1. Anatomical description

We assume that the main role of the eardrum is to ensure energy is efficiently transmitted from the ear canal to the OC. The impedance of the OC is significantly higher than in the canal (our study assumes a factor of 30 (Bekesy and Rosenblith, 1951; Zwislocki, 1957)), thus a direct interface would result in a near-total reflection and large standing waves. The TM has a conical funnel shape, its mouth toward the ear canal and its throat toward the OC (umbo). It is set at an angle with respect to the ear canal axis which varies significantly between species; for the cat it is roughly 40° (Fay, 2001, p. 17), as shown in Fig. 2(a). Lim (1968a,b); Funnel and Decraemer (1996) and others have detailed the geometry of the TM, its microstructure, and its different layers of fibers. The general idea is that these layers, along with the double curvature of the funnel, are responsible for the membrane stiffness (and impedance). To ensure a proper impedance matching, the TM characteristic impedance increases continuously, starting from values close to the canal impedance at its periphery, to much higher values at its center. Propagation of the vibration is realized by transverse waves on the TM surface, coupled to the compressional airborne waves in the canal. Previous works have highlighted that the TM brings an important delay; estimates from Olson (1998) and from Puria and Allen (1998) have shown it is on the order of 30–40 μs: thus, the TM can be seen as a delay line, with a space-varying characteristic impedance to match the air and OC waves. Given this view, the TM is similar to an acoustic horn. Note that this TM horn-like propagation does

not occur in air, but rather as a transverse wave, which is a significant difference when compared to previous theoretical works on traditional acoustic horns (Beranek, 1954; Salmon, 1946a,b).

2. Distributed model

The essence of this contribution is inspired primarily by previous research on high-frequency middle ear models (Shaw, 1977; Goode and Killion, 1987; Puria and Allen, 1998). The *first* goal is to identify the key factors in the interaction of the airborne canal compressional wave and the membrane-borne TM transverse wave. Our *second* goal is to implement a time-domain, reflectance-based (Kelly and Lochbaum, 1963) model simulation of this "canal ⇔ TM" wave interaction. Since this is the first attempt at such a detailed interaction model, many shortcuts and approximations are necessary. It is hoped that any shortcomings and limitations can be the work of future models.

Although it is neither circular nor symmetrical, the TM can roughly be seen as a very shallow horn, and to a further extent as a plane circular membrane if we neglect its depth with respect to its diameter. This assumption is valid for the range of frequencies we shall consider (0.3–15 kHz), where the wavelength is much larger than the TM dimensions; in Fay (2001, p. 21)) the cat's TM depth is estimated to be around 1 mm while our study focuses on wavelength ranging from 7 to 350 mm.

The TM is discretized into N concentric annuli, each having a *characteristic impedance* that gradually increases, from the periphery to the center. Figure 2(b) shows an example of this first decomposition, for $N=5$; the figure shows only a small number of annuli for the sake of simplicity: actual simulations were obtained with $N=71$ (i.e., 14 times more). This representation, a significant approximation of the TM, requires two-dimensional processing of the wave; in fact, due to the tilt of the TM in the canal, different locations on a given annulus will not contact the canal wave at the same time. Properly modeling the synchronization of the different locations seems a difficult issue and so the model is further simplified, with this circular model a conceptual stepping stone to the model shown in Fig. 2(c).

In order to work in one dimension, the circular model (Fig. 2(b)) is replaced by the rectangular model (Fig. 2(c)). As the airborne canal compressional wave touches the TM, the compressional transverse membrane-born wave is impressed into the TM membrane. It is assumed that the impedance match between the airborne sound and the transverse elastic membrane-born sound is such that most (but not all) of the energy is coupled into the membrane. If this were not the case, all energy would be reflected back into the canal, which is not the experimental observation: in actuality, some energy is reflected, but most of it is propagated to the OC. This coupling of energy requires the conservation of mass and momentum (Kirchoff's laws). Thus the volume velocity is scaled in the spatial domain to ensure mass conservation, by taking into account the relative area of the annuli, so that larger annuli (at the periphery) are given more weight than central annuli. This results in the representation of Fig. 2(c), where one stripe corresponds to one semiannulus in Fig. 2(b). If A_i is the area of the stripe at index i, and r_i its radial position, referenced from the TM center, then

$$A_i = \frac{\pi(r_i^2 - r_{i-1}^2)}{2} \simeq \pi r_i \Delta r_{tm}, \tag{8}$$

where Δr_{tm} is the annulus width. Note that the central stripe has the same area as the central disk in the annular discretization. Thus, N annuli are associated with $2N-1$ stripes on the TM. Also, symmetrical positions with respect to the umbo represent the same single annulus, hence they are characterized by the same impedance. Note that it is an even coarser representation than the circular discretization of Fig. 2(b). Following sections of this paper show, however, that it is relevant. In actuality, the impedance varies continuously from the periphery to the umbo and so we assume that reflections occurring during transverse propagation on the TM are negligible (this is the second of the limitations mentioned above, that could easily be repaired, given the motivation). As a consequence, in this model, once the wave has been transmitted onto the TM from the canal, it is *not* reflected anymore and propagates unaltered to the umbo. On stripe i, the TM is then modeled by a pure delay corresponding to the distance to the umbo. Each stripe is then modeled by: 1) a reflection coefficient from the interface with the canal, 2) a pure delay, represented by a double (forward/backward) radial transmission line. With this representation, the stripes are totally independent from each other and they do not interact.

3. Reflection coefficient function

The main issue is to derive an impedance function for the TM in order to associate each TM transmission line with a reflection coefficient from its interface with the ear canal. This derivation is obviously not trivial and is one of the key contributions of this analysis. From Sec. II, each semiannulus (stripe) of the membrane can be represented by a series $Z(s)$ and shunt $Y(s)$ association, where $Z(s)=\rho s$ (ρ is the annulus density, which we use here because we consider an infinitely small volume) and $Y(s)=Cs$ (C is the annulus compliance brought by the membrane's curvature). The basic hypothesis of the model is to assume impedances are invariant on the annulus, i.e., there is no assumed space dependency other than that of the natural annulus area variation (a third significant simplification). The characteristic impedance of the semiannulus number i is then, from Eq. (6)

$$z_0^i = \sqrt{\frac{\rho_i}{C_i}}. \tag{9}$$

We have not found empirical estimates of this compliance in the literature, however another equivalent variable can be more intuitively considered: the speed of sound, $\mathcal{C}$, defined as

$$\mathcal{C} = \frac{s}{\gamma(s)} = \frac{s}{\sqrt{Y(s)Z(s)}} = \frac{1}{\sqrt{\rho C}}. \tag{10}$$

Given an estimate of the density and speed profiles along the membrane, one may then compute the TM impedance at each location. Such profiles, however, are still not readily available to the authors, and would be complex to implement

(a good exercise for the future). The impedance function used in the model then relies on two more hypothesis: (1) the wave speed is constant over the entire TM surface and (2) the impedance profile is exponential. The constant speed hypothesis may well be wrong: previous works strongly suggest that it is not verified on the whole surface (Funnel and Laszlo, 1978; Rabbitt and Holmes, 1986; Funnel *et al.*, 1987; Rosowski *et al.*, 2006). However, our model does not aim at describing the subtleties of the TM 3D motion. Thus we have assumed a constant speed derived from simple delay estimates, the rationale being that such an approximation would be nearly transparent from the input impedance point of view, on which the whole work is based. As for the impedance exponential profile assumption, we have previously suggested that it is probable that some analogies do exist between the traditional acoustic horn theory and our TM model: we have then assumed a simple, classical profile to start our derivation. Thus, the impedance of annulus i assumes the form

$$z_0^i = z_0 e^{-2\mathcal{M}r_i}, \tag{11}$$

where z_0 is the impedance at the umbo, r_i is the radial position on the membrane, with the origin at the center, and $\mathcal{M}$ the flair constant. It is defined from the radius and the impedance transformer ratio of the TM:

$$\mathcal{M} = -\frac{1}{2r_{tm}} \log\left(\frac{1}{\text{Ratio}_{tm}}\right). \tag{12}$$

Our study assumes an impedance transformation ratio of 30 for the global system including the TM and the OC. It is commonly assumed that the OC performs a transformation due to its lever ratio, $N_{\ell r} \approx 2$ (Puria and Allen, 1998), probably due to rotation about the incudo-malleolar (IM) joint (Guinan and Peake, 1967). The impedance transformation realized by the TM alone is then

$$\text{Ratio}_{tm} = \frac{30}{N_{\ell r}^2}. \tag{13}$$

Note that $N_{\ell r}$ represents the ratio of malleus to incus *displacement*, which is why it is squared in the *impedance* ratio computation. The TM reflection coefficient function $\mathcal{R}_{tm/ec}$ can then be computed from the canal impedance, being aware that it depends on its position along the axis; in fact, the canal cross-section area gets smaller and smaller toward its termination, due to the TM inclination. This model leads to very large impedances at the canal termination, resulting in reflection coefficients being close to −1 and too much reflection at the interface. Thus, we have decreased the negative reflection coefficients (by 70%) to eventually obtain the reflection function shown in Fig. 3. Note that it is asymmetric, due to the TM inclination and the resulting impedance variation in the canal.

Reflection coefficients are more intuitive to deal with than impedances. That is why our approach was

1. to derive an impedance function on the TM,
2. then, to compute the corresponding reflection function due to the interface with the canal, and finally
3. to adjust the negative reflection coefficients via experimentation.

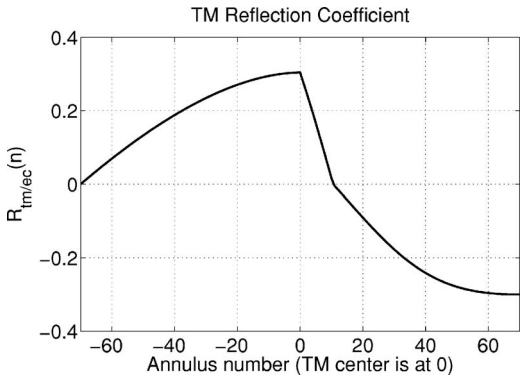

FIG. 3. Tympanic membrane reflection coefficient for a discretized membrane with 71 annuli, i.e., 141 samples. Note the asymmetry in $\mathcal{R}_{tm/ec}$, and its maximum, at the TM center. At the canal termination, the canal impedance is actually greater than the TM impedance, which results in negative reflection coefficients.

It is difficult to justify our final adjustment in terms of TM impedance, but the resulting reflection function seems physical, as is shown from simulations. In our analysis, the previous TM impedance description may not be not an accurate model, but rather viewed as a pedagogical stepping stone to obtain a relevant reflection function.

4. Interface with the ear canal

As in the ear canal model, the number of annuli N is based on the sampling rate f_s and from the wave speed on the eardrum. Both theoretical considerations as well as delay estimates (Olson, 1998; Puria and Allen, 1998), require that the speed of sound on the membrane, $\mathcal{C}_{tm}$, is slower than in the canal by a factor we shall call q, provided in the table of constants. Defining Δr_{tm} as the annulus width, i.e., the spacing between positions on the TM, we then have

$$\mathcal{C}_{ec} = q\mathcal{C}_{tm}, \tag{14}$$

$$\Delta x_{ec} = q\Delta r_{tm}. \tag{15}$$

As a consequence, it is impossible to line up every TM transmission line input with a canal sample. Our solution to this problem is to up sample to improve the density of samples on the TM. The classic up-sampling method consists in padding with zeros and low-pass filtering (Oppenheim *et al.*, 1999). This is not possible here because q is not integral. To solve this problem of fractional delay, we perform two operations. First, we up sample to reduce the size of a sample delay. Second, we model the delay from each TM annulus to the OC independently of the other sections, as summarized in Fig. 4. At location i_0 on the TM, the canal forward wave is scaled by

$$w_{i_0} = \frac{A_{i_0}}{A_{tot}}, \tag{16}$$

where A_{i_0} is the area of stripe i_0, computed from Eq. (8) and $A_{tot} = \Sigma_{i=1}^{2N-1} A_i$ is the TM total area. The wave propagates in air under the TM (first transmission line) and then hits the

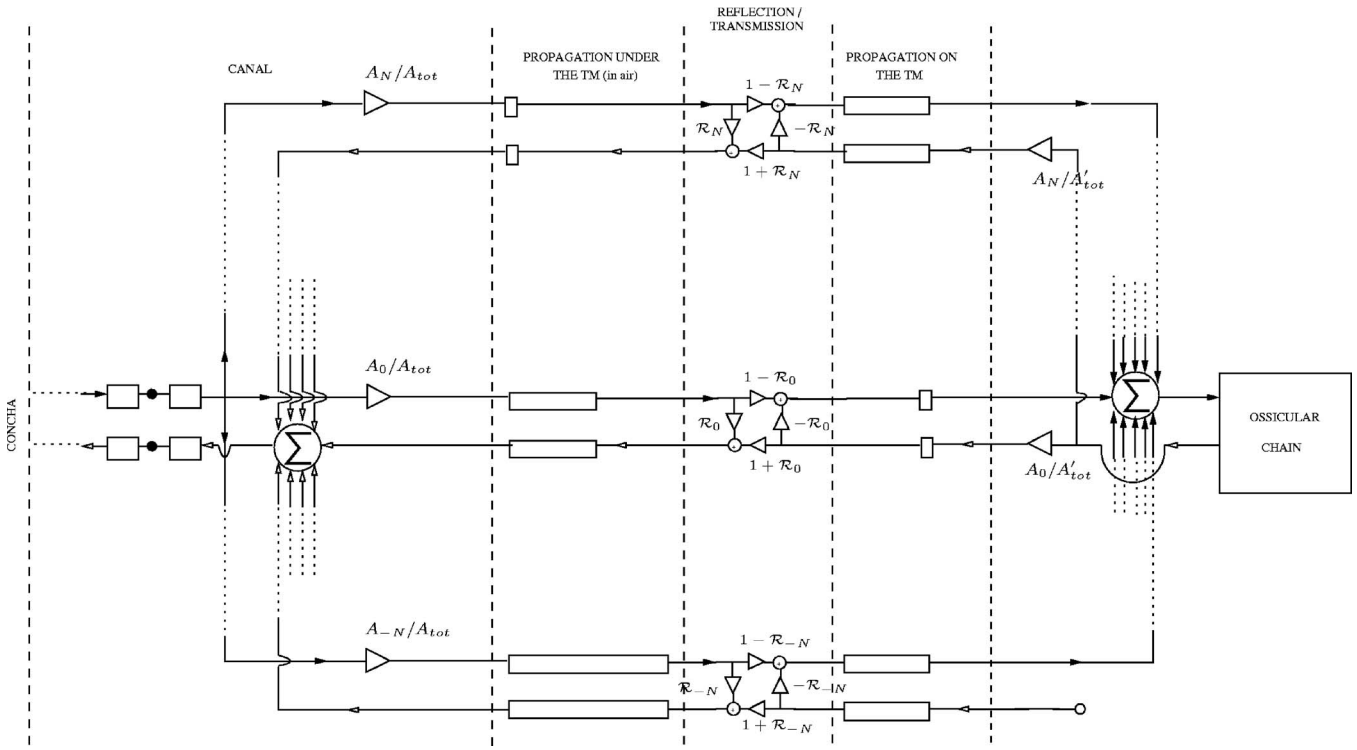

FIG. 4. Interface between the ear canal and the tympanic membrane. Forward and backward propagation path are represented by solid and hollow arrow heads, respectively. Rectangles represent transmission line delays with length proportional to delay. In the first section from the left, at the canal termination, the last forward sample is multiplexed into the interface transmission lines and scaled according to the ratio of the stripe area A_i over the total TM surface area A_{tot}. The second section from the left represents transmission lines showing the wave in air under the TM; due to the inclination of the drum, they bring different delays. At the interface between the canal (air) and the membrane (the middle or third section), the wave is split into a transmitted and a reflected part, computed from the knowledge of the reflection coefficient on the TM (see Fig. 3). In the fourth section the transmitted part propagates on the TM toward the umbo (right-most series of transmission lines) where finally, in the fifth section, all contributions are added and then feed the OC. The reflected part at the canal/TM interface propagates in air back to the canal input. In the backward propagation, the wave coming from the OC is only input into the TM superior region, where it is in contact with the manubrium, and is multiplexed and scaled according to the ratio of the stripes areas over the superior region area, A'_{tot}. It propagates to the canal input using the same path than the forward-going wave. All contributions are then added before being input into the canal transmission line. Note that our actual implementation takes into account the future possibility of adding an input from the middle ear cavity space into the inferior region, but these (velocity) inputs are presently zeroed (far lower-right corner).

TM. At that point, it is split into two contributions: one transmitted on the TM, and the other reflected into the canal. The reflection coefficient, $\mathcal{R}_{i_0}$, is different at each location on the TM and has been derived in Sec. III. Since $\mathcal{R}_{i_0}$ is frequency independent, transmitted and reflected contributions are simply computed by a multiplication:

$$\begin{bmatrix} u^-(x) \\ u^+(x+dx) \end{bmatrix} = \begin{bmatrix} \mathcal{R}_{i_0} & 1+\mathcal{R}_{i_0} \\ 1-\mathcal{R}_{i_0} & -\mathcal{R}_{i_0} \end{bmatrix} \begin{bmatrix} u^+(x) \\ u^-(x+dx) \end{bmatrix}. \quad (17)$$

Both transmitted and reflected parts propagate in their respective medium, toward the umbo or the canal termination where they are summed up and fed to the single-transmission line representation used in the OC and in the canal, respectively. At the umbo, the impedance is matched with the OC and we assume that waves are entirely output to the OC, and that they do not propagate to the other side of the TM. This is actually quite intuitive given the conical shape of the TM.

The backward-going wave, reflected from the OC, uses a similar path in the opposite sense. Along the OC, we assume a transverse propagation of the wave. As a consequence, the OC applies a force on the TM superior region, along the manubrium. Note that it is different from the interface between the TM and the canal: in the canal, we assume the sound wave to be compressional in air and in contact with the TM over its entire surface. Due to the independence of the annuli transmission lines, the inferior region of the TM does not play a role in the backward propagation of the wave. Note that the middle ear cavity space has a compressional wave in air which will apply a pressure over the entire TM. We have presently chosen not to model this phenomenon; however, our current implementation is ready for such an extension. As indicated in Fig. 4, all inputs of the inferior region for the backward-going wave are set to zero but could receive a different input in a future development of the model.

5. Power conservation

It is important to discuss power conservation at this point, as it is necessary for the validity of the model. Two operations are involved in the process of propagation: the spreading of the wave from the canal termination (and from the OC input) to the TM and the reflection junction at the interface between the canal and TM transmission lines. The spreading of the wave is designed to conserve volume velocity (the sum of the scaling factors is 1) and so the operation is equivalent to connecting a duct into a series of smaller

ducts which cross section areas sum up to be equal to the bigger duct cross section area, which does conserve power. As shown by Bilbao (2001), the reflection junction also conserves volume velocity. Thus the middle ear model, as implemented, is lossless.

B. Ossicular chain

1. Anatomical description

The OC is an association of three bones coupling the TM output and the cochlea oval window. Complex mechanical interactions between them and their ligaments act as a lever from the input of the chain to its output: as a consequence, the impedance is increased with minimal sound reflection. Note that this is also an impedance matching process, but lumped rather than distributed. This description as a lever, while valid at low frequencies, breaks down at higher frequencies due to the OC mass. A more refined high-frequency description is beyond the scope of this study and we have assumed, as in (Puria and Allen, 1998), that the lever ratio was constant over the entire frequency range of interest.

After having propagated along the TM, the wave reaches the umbo, where it is connected directly to the malleus manubrium tip. In actuality, the manubrium is connected to the TM along the entire length of its superior region. The wave then propagates through the OC, and arrives at the stapes footplate, a flat piece of bone embedded in the cochlea oval window and fixed by the annular ligament. The footplate moves in the oval window, transmitting the vibration to the cochlea fluid, and in reverse for the retrograde wave. The various lumped elements make up a transmission line, having series mass and shunt stiffness, with a characteristic impedance given by Eq. (6).

2. Lumped-parameter OC model

The middle ear model shown in Fig. 5 is largely inspired by the circuit presented by Puria and Allen (1998), which in turn is based on the work by Zwislocki (1957). The lumped-parameter circuit for the OC representation has proved to be a modeling method which is easy to implement and accurate (Brillouin, 1953; Zwislocki, 1957, 1962; Lynch *et al.*, 1982; Puria and Allen, 1998). This method has been implemented in the time domain, to be used with the TM model.

Generally, bones are represented by mass (inductance) and ossicular joints by springs (compliance): the OC is then a sequence of mass/compliance shunt associations. The reason for this is suggested by Puria and Allen (1998): to increase the bandwidth of lumped-parameter circuits, each mass is coupled with a shunt compliance; in such an association, the two-port characteristic impedance does not depend on frequency (the dependencies in s cancel out) and compliance can be adjusted given the mass, so that the impedance is matched. Each two-port is defined in the time domain by the four frequency-dependent reflectance filters described in the caption of Fig. 5, from which the outputs are computed. A detailed description of these reflectance filters' computation is not provided here, other than to say that the "ABCD matrix" method (expression of output velocities from input velocities) and the bilinear transform were used. Note how the OC lever ratio is represented by a transformer between the malleus and the incus. Its ratio is denoted $N_{\ell r}$ and the malleus and incus impedances are related by $Z_i = N_{\ell r}^2 Z_m$. The OC implementation details are provided in an appendix.

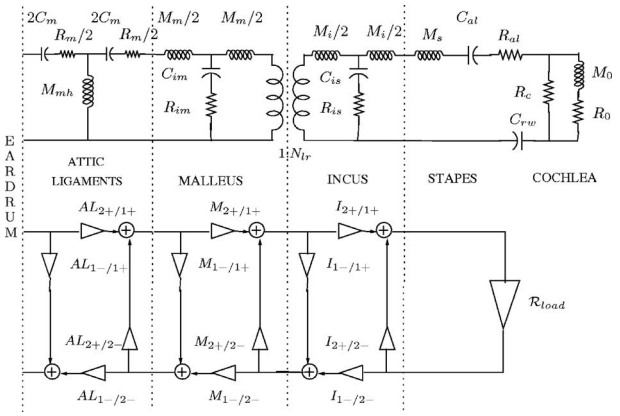

FIG. 5. Ossicular chain circuit representation. Each element is modeled by a two port with four filters given by the matrix of Eq. (17). The multipliers are frequency-dependent, and thus must be implemented as convolutions in the time domain. This is done using a bilinear transformation of the reflectance function in the frequency domain. this operation converts the Laplace-domain formula into its digital domain (Z—transform) equivalent. It replaces the Laplace variables s by $2fs(1—z)/(1+z)$, where fs is the sampling rate. $X_{2+/2-}$ represents the filter computing the forward output from the backward input, $X_{1-/1+}$ the backward output from the forward input, etc. The stapes/cochlea association is modeled by only one filter (Lynch *et al.*, 1982). The OC lever ratio is represented by the transformer between the malleus and the incus, its ratio is denoted $N_{\ell r}$. Malleus impedance Z_m is matched with the TM central impedance, and incus impedance is equal to $N_{\ell r}^2 Z_m$.

IV. RESULTS

Various simulations are run with the model described previously, and the results are compared to experimental conditions, to check for consistency against normal as well as pathological conditions. These comparisons are then used to refine the model parameters, starting from (Puria and Allen, 1998). Once the parameters are established for each section, no further changes are made to that section. At each stage the model is compared to experimental data. Finally the entire model is compared to the ossicles displacements ratios of Guinan and Peake (1967).

A. Impedance-related measurements

Impedance measurements by Allen (1986) are used to determine the model parameters. Following the approach by Zwislocki (1962), simpler cases are studied first, such as the blocked TM, and the disarticulated stapes, in order to reduce the number of unknowns. The complexity of the model is then incrementally increased, with the previously adjusted parameters fixed.

1. Case I: Blocked tympanic membrane

The simplest case (Fig. 6) is the input impedance of a blocked umbo, i.e., loaded by an infinite impedance at its output ($\mathcal{R}_{\text{umbo}}=1$). This condition is necessary as it is used to adjust the TM reflection coefficients. The results of Fig. 6

show the expected characteristics of a pure delay transmission line, corresponding to the residual canal and TM delay. As a sanity check, this delay can be estimated from the output of the TM. In Fig. 6(b), the main pulse occurs at 40.43 μs. Subtracting the canal delay of 4.32 μs (length of 0.15 cm), the TM delay estimate is 36.11 μs (estimate by Puria and Allen (1998) is 35.7 μs for the ear on which this model is based (p. 3476). Their estimates for the other two ears are 34 and 41 μs (p. 3472)).

The general shape of the output signal (Fig. 6(b)) can be roughly approximated by two consecutive broad, dispersed pulses: the first one (the greatest) corresponds to the propagation of the wave coming from the superior region of the TM, and is followed by the wave propagating on the inferior region. Some noticeable "perturbations" occur periodically in the fine "structure" of the signal, especially for the inferior region wave. This is due to the discrete TM implementation that was used: for each location on the TM, the corresponding canal+TM delay is rounded to be a multiple of the sampling period, which leads to the signal not being perfectly continuous at the umbo. Those perturbations do not have any influence over the general behavior of the system, as is seen from the impedance plots. Actually, given a physical measurement of the blocked TM response, one would not see the discrete pulses, which are an artifact of the discrete nature of the TM model, as any low-pass filter effect would remove them. The time reflectance shows three broad consecutive pulses. The first two pulses (at 18.19 and 41.44 μs, respectively) show the same periodical perturbation that we previously discussed: the first one corresponds to the primary reflection of the wave on the superior region of the TM where reflection coefficients are positive, the second one corresponds to negative reflections in the inferior region. Eventually, the propagated signal is reflected by the blocked condition and appears as the third broad main pulse (at 71.26 μs).

Figure 6(c) presents the reflectance magnitude: it reveals a slight decrease of the high frequencies, above 15 kHz, where it crosses 0.8. Since the line is lossless, this phenomenon is nonphysical. Our hypothesis is that the spreading of the wave and the various delays at the canal/TM interface lead to the reflected signal at canal input being similar to a sequence of pulses (see Fig. 6(a)), which Fourier transform rolls off at high frequencies. We believe that, in actuality, a more complex phenomenon (or a combination of such) takes place along the path of propagation which compensate for this high-frequency loss. A probable candidate for such a phenomenon is the interaction between the TM transmission lines. We have assumed no reflection occurred on the TM, which is an approximation: it is possible that such reflections do exist and have a noticeable influence at high frequencies. The model as implemented is therefore not accurate above 15 kHz. The impedance plot of Fig. 6(d) is characteristic of a blocked transmission line with acute poles and zeros, since no damping is assumed. The previously mentioned high-frequency reflectance decrease is also visible in the impedance magnitude's less acute pole around 15 kHz, although less obvious.

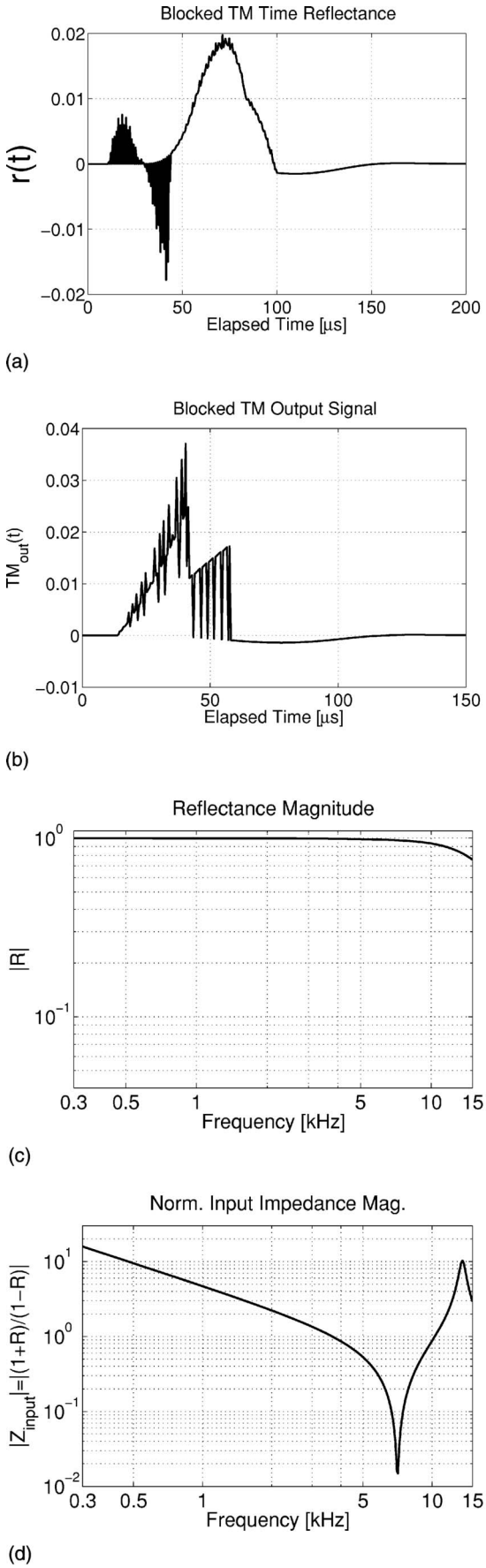

FIG. 6. Tympanic membrane for the *blocked-TM* (clamped-umbo) condition: time-domain reflectance and TM output, reflectance and impedance magnitudes. (a) Reflectance (time signal), (b) TM output, (c) reflectance magnitude, (d) impedance magnitude.

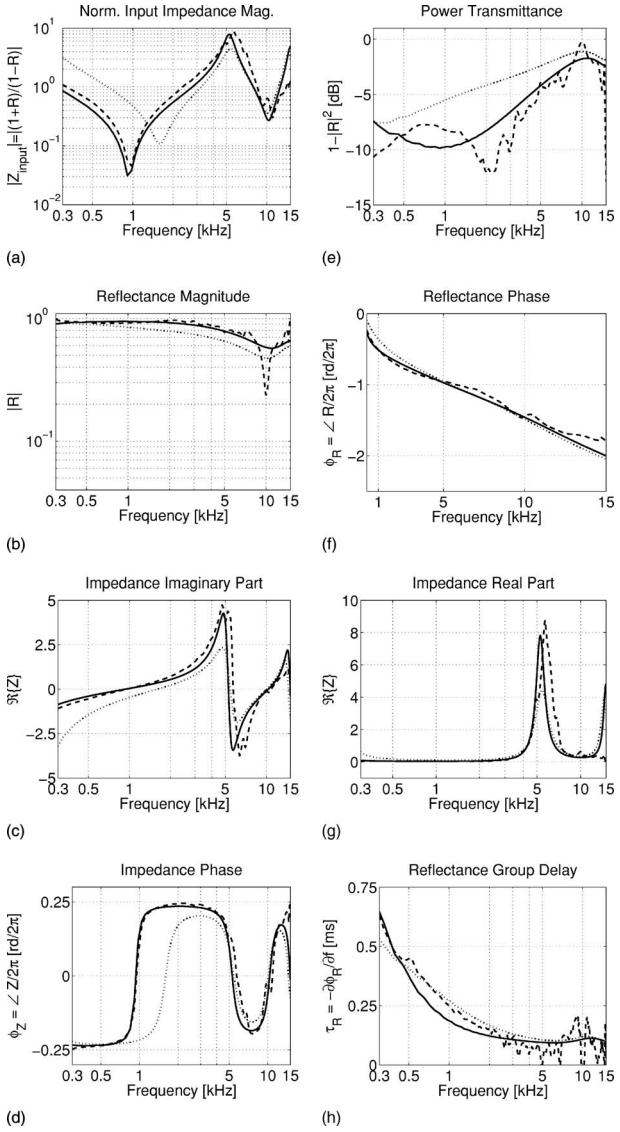

FIG. 7. In this figure we compare the experimental data for the disarticulated stapes (DS) [dashed] with two model simulations, the disarticulated stapes (DS) [solid] and the drained cochlea (DC) [dotted]. In the left column are four input impedance measures: (a) the impedance magnitude, (b) the reflectance magnitude, (c) the impedance imaginary part, and (d) the impedance phase. In the right column are: (e) the power transmittance, (f) the reflectance phase, (g) the impedance real part, and (h) the reflectance group delay. As discussed by Allen (1986), removing the stapes reduces the stiffness below 1 kHz by about a factor of 3, as shown in (a) for the model calculations, but otherwise has only a small effect, especially above 5 kHz.

2. Case II: Pathological ears

Figure 7 displays the results obtained with the model, compared with experimental data from Allen (1986), for the disarticulated stapes (DS) experiment. In this case, the ossicular chain is cut free just before the incudo-stapedial (IS) joint, corresponding to a short circuit (the load impedance is zero), resulting in $\mathcal{R}_{\text{incus}}=-1$. The DS experiment is important for adjusting the attic ligaments parameters, C_m and R_m, as well as the malleus parameters, M_m, C_{im}, and R_{im}. The intuitive behavior of the system is confirmed by the experimental data (dashed line) and the results of the model (solid line). The impedance magnitude has acute poles and zeros, characteristic of low-loss standing waves. A significant difference between the DS data (a) with respect to a normal short-circuit transmission line, is the low-frequency stiffness response below 1 kHz, confirmed by the phase response (d). Namely, the short circuit line has a zero at $f=0$, whereas the middle ear, in short circuit, has a pole. Such a stiffness most likely results from the attic ligaments. In the model this stiffness results from C_m. The irregularity in the experimental resistance in (g) is due to the inherent difficulty in measuring a relatively small resistance in the presence of a large stiffness (i.e., the impedance angle is very close to −90°). Also are shown the reactance (c) and reflectance phase (f).

The reflectance is shown (b). It is less than 1 because of the OC losses. The power reflectance part (e) shows the relative low power transmitted into the disarticulated middle ear. Below 2 kHz, the experimental data show a slight increase of the transmittance from −10.5 to −8 dB between 300 and 700 Hz, then a plateau up to 1.5 kHz, and a sharp decrease down to −12 dB at 2 kHz. This behavior is not captured by the model which first decreases from −7.5 to −10 dB between 300 Hz and 1 kHz, and then increases up to 10 kHz. However, the model remains within ±3 dB of the experimental data, except perhaps around the sharp minimum at 2 kHz; (h) gives the latency of the reflectance, a measure of how long the energy remains in the middle ear. The low-frequency slope of the model is slightly smaller than for the experimental data, highlighting that the model stiffness is also slightly smaller, which is confirmed by the impedance magnitude in this region. Around 10 kHz, the experimental group delay shows a local maximum which is not present in the model simulation: this discrepancy is probably due to the least inaccuracy of the model at high frequencies, as suggested from the blocked-TM results.

In the next stage of analysis we add back the stapes and annular ligament, as well as the cochlea model. In Fig. 7 (dotted lines), are shown model results from the case of the drained cochlea (DC). In this case the experimental data are not shown, to reduce the clutter, and because the difference is easily described. In the DC experiment, the entire OC is left intact but the cochlear fluid is drained, resulting in a great reduction of the cochlear load (stapes volume velocity is basically unloaded). From the data of Allen (1986), the canal impedance is very similar to the DS experiment, except for an increase in the stiffness below 1 kHz, due to the inclusion of the annular ligament. This change can also easily be seen in the real and imaginary parts of the impedance, in Figs. 7(c) and 7(g). The difference is mainly visible at low frequencies, and not at all above about 4 kHz, except for a general decrease of the impedance magnitude because the middle ear is better matched to the canal in this case. Note how the resistance increases over most of the frequency range. At 5 kHz this is difficult to see due to the large peak in the resistance, associated with the pole in the impedance.

3. Case III: Intact ear

With the intact ear, the change from the two previous cases is dramatic, although the main difference in the model is the cochlear resistance, previously equivalent to an air load. The consequence of this highly resistive final load, matched to the middle ear output, is a dramatic damping of

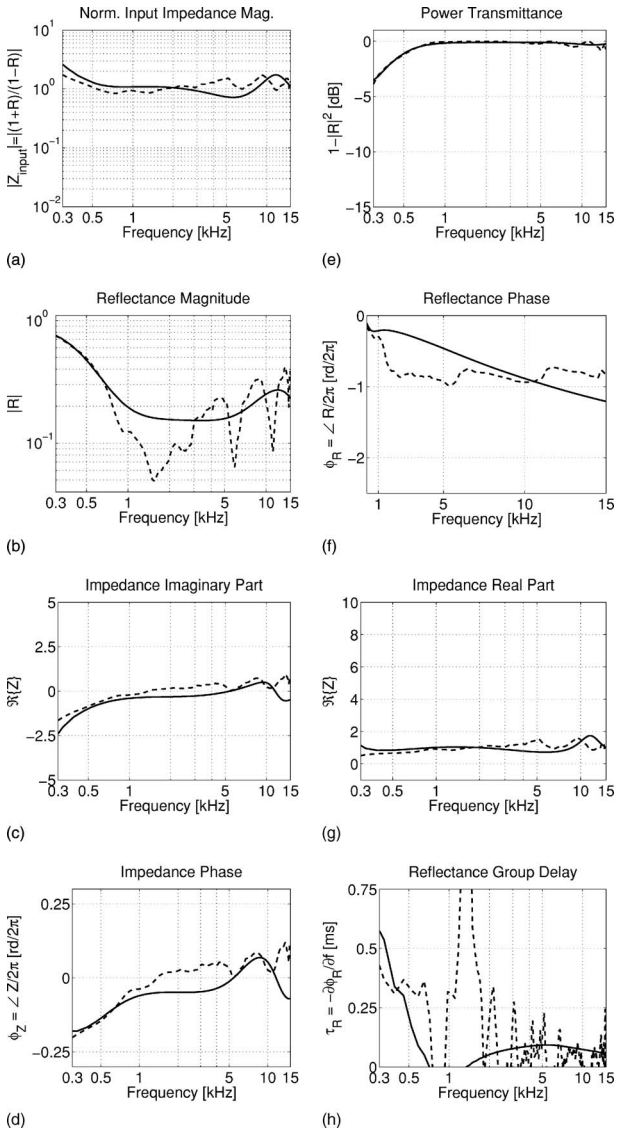

FIG. 8. In this figure we compare the experimental data for the intact ear [dashed] with the model simulation [solid]. In the left column are four input impedance measures: (a) the magnitude impedance, (b) reflectance magnitude, (c) the impedance imaginary part, and (d) the impedance phase. In the right column are: (e) the power transmittance, (f) the reflectance phase, (g) the impedance real part, and and (h) the reflectance group delay. The intact ear brings a major change with respect to the pathological ears: due to the increased load impedance, standing waves are damped out and reflectance is much lower, overall.

the standing waves, and the reflectance being globally much lower, as shown in Fig. 8. From the impedance plot, the damping is obvious since the phase of the impedance is close to zero, above 1 kHz.

The overall match to the experimental data is generally excellent. A more detailed study of the impedance real and imaginary parts, Figs. 8(g) and 8(c) shows some small discrepancies. The low-frequency slope of the impedance is due to the stiffness of the system: it can be seen from Fig. 8(a) that the model is slightly stiffer, which results in too high an impedance and group delay. Above 1 kHz, experimental data show that the resistance slightly increases, while the model is less resistive (Fig. 8(g)). Also, the ear becomes slightly mass dominated, as can be seen from the phase plot in Fig. 8(d) and the imaginary part in Fig. 8(c). This has obvious consequences on the impedance and reflectance between 1 and 5 kHz: Figs. 8(a) and 8(b) clearly show the model is not as well matched as the actual ear. Between 5 and 10 kHz, experimental data show resonances (standing waves) which are not captured here. Above 10 kHz the ear is still slightly mass dominated, while the model has a slightly negative imaginary part for the impedance. Another serious discrepancy can be seen in the reflectance phase in Fig. 8(f) around 1.2 kHz, the measured phase suddenly drops from -0.3 to -1 rad$/(2\pi)$ which can also be seen as the notch in the reflectance plot. More generally, the complex reflectance is characteristic of a series of delayed pulses with different phases and magnitudes, which results in the several notches in the magnitude and the sawtooth-like behavior in the phase. The model, however, remains smooth. This is even more obvious in the group delay plot (Fig. 8(h)) which shows a huge peak at 1.2 kHz, due to the phase discontinuity. Also, the low-frequency group delay is nearly constant while our simulation is progressively decreasing. This behavior probably shows a shift of mode between the stiffness-dominated low-frequency region and the mid-frequency range which is more resistance dominated: the change is very sharp in the actual ear while the model seems to smooth out the transition. Modes transitions are quite difficult to appreciate and our model is probably too simplistic to deal with them accurately (Fay *et al.*, 2006).

Despite those numerous discrepancies, the model matches the data fairly well, and the general behavior of the ear is nicely captured. As the agreement is clearly less good than with the pathological ears, a probable source for the discrepancies is the lack of a cochlea model. Simulations run with the stapes/cochlea filter on its own, using Lynch's values give excellent agreement with his results. However, clear differences appear when it is used with the global TM-OC system since it requires significant adjustments to match experimental data, especially for the helicotrema parameters. Our hypothesis is that the model by Lynch has been derived using measurements made by direct stimulation at the stapes footplate, hence bypassing the entire TM and OC. We have tried to compensate such a major difference by multiplying the impedances by Ratio_{TM}, which seems to be relevant for most parameters except the helicotrema. We suspect that impedance transformation is not the only process involved in the interaction between the OC parameters and the cochlea and it is possible that the current circuit is too coarse to deal with such processes accurately.

B. Ossicles displacement ratios

An ultimate validation of the model is carried out by comparing its results to data which have not been used at all in its derivation. Guinan and Peake (1967) measured ratios of displacements in the OC (slippage). These are taken to be classical references of the ear typical behavior. This comparison is shown in Fig. 9. In general, the model is in good agreement with the experimental data, except for the high-frequency phase of the incus to malleus displacement. This discrepancy is actually the exact same as the one reported by

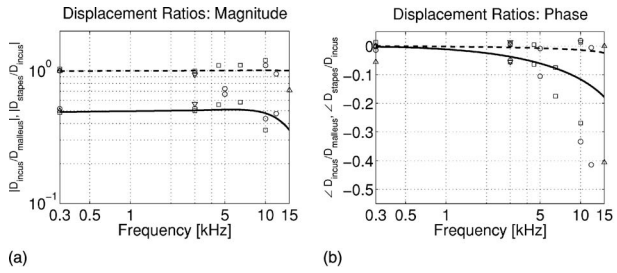

FIG. 9. Ossicles displacement ratios: magnitude and phase. The model incus to malleus displacement ratio is the solid line, the model stapes to incus displacement ratio is the dashed line, symbols are cats 58, 65, 68, and 69 from Guinan and Peake (1967). (a) Ratio magnitude, (b) ratio phase.

Puria and Allen (1998): since the model uses their parameters values, it is not too surprising and actually underlines the consistency of our time-domain approach. This phase difference merely represents a delay difference. It is possible that an additional slippage factor is involved at the IM joint which could have an influence on the phase. Such a factor was used in the work by Puria and Allen (1998, p. 3471) but its influence is not obvious and, in any case, it did not bring any improvement here.

V. DISCUSSION

The model gives a robust match across all conditions. However, some discrepancies in the middle ear model need to be refined, especially at high frequencies, above 10 kHz. Further refinements will require an improved cochlear load simulation. This study leads to two significant results. The first one is the relevance of the time-domain implementation, a very intuitive and convenient approach, and, in our view, certainly useful to model distributed and/or nonlinear systems, such as the TM (and the cochlea). The second is the added insight that the time domain provides into the basic operating of the TM and its impedance-matching properties; in our view this approach provides a different way to look at the TM, and to appreciate how wave propagation occurs and how the different delays interact.

A. Attic ligaments

Experimental data for the disarticulated stapes experiment show the presence of a stiffness element in the ear, before the annular ligament. It can be assumed that the IM- and IS-joint ligaments do not add stiffness to the input impedance, as the joints are compensated by the ossicles mass, associated with them (matched-impedance transmission line condition). It is probable that this stiffness results either from the TM, or the attic ligaments. Puria's model—and consequently this study—assumes the attic ligaments are responsible for this low-frequency stiffness: such an assumption is relevant and both models show reasonable agreement with this hypothesis. It is open to question, however, until it is experimentally verified; in fact, from the input impedance point of view both approaches are quite equivalent and our model is not able to partition between them. At the junction between the umbo and the malleus and at the IM joint, the bone movements are mainly rotational. Thus, it can be assumed that the ligaments are not significantly stretched: they mainly have a "ball-bearing"-like behavior, bonding the ossicles to the attic, rather than being stretched. Alternatively, it seems reasonable to think the TM, with its many layers of microfibers, brings stiffness to the system. This is entirely an experimental issue.

B. Tympanic membrane cutoff

The impedance-matching role of the TM is widely recognized. Various hypothesis have been suggested to explain this role, such as the TM/footplate area ratio, but the hypothesis here is that this match is realized thanks to a radially varying impedance. From theoretical studies, nonhomogeneous media lead to evanescent modes (Salmon, 1946a,b; Leach, 1996): below a certain cutoff frequency, no energy is propagated because the propagation factor γ is real (see Sec. II). To our knowledge, such evanescent waves propagation in the middle ear has never been investigated. We feel this problem needs further experimental and theoretical investigation, with some priority.

VI. SUMMARY

This research has been focused on implementing a time-domain model of the middle ear, and is a significant extension of the frequency domain model of Puria and Allen (1998) in that the ear canal and the tympanic membrane are represented by a parallel complex of delay lines; their interface is complex due to the inclination of the membrane in the canal, due to different speeds of sound in both media, and due to the impedance mismatch between the two. Using a particular spatial distribution, the transmission from one to the other is simulated and the reflection is computed using an exponential TM impedance distribution. Simulations show good consistency with the model.

The TM system is then coupled to a time-domain version of the previously published lumped-parameter model of the middle ear (Zwislocki, 1962; Puria and Allen, 1998). Ossicles parameters are adjusted manually from published values in order to match experimental data in three cases: disarticulated stapes, drained cochlea, and intact ear. The final adjusted model shows relevant similarities with impedance-based and ossicle motion measures.

The model does an excellent job of capturing the essence of the middle ear responses. Some discrepancies still exist at high frequencies, especially in our highly simplified cochlear load impedance, and underline the need for some refinements.

Relative to previous studies, the new model offers two main differences. While previous works have modeled the middle ear in the time domain (Funnel and Laszlo, 1978; Rabbitt and Holmes, 1986; Funnel *et al.*, 1987), as far as we know, no such "wave" models have been published. Our wave formulation allows for significantly more detail in the TM model and for the simulation of wave propagation on its surface. With respect to previous detailed models, the main interest is to be able to directly observe the spreading of the wave on the TM surface by modeling its time response. Second, the TM distributed model enables better simulation of its complex interface with the ear canal and its space-varying

impedance distribution. We show that it interfaces to existing OC models easily, and offers interesting agreement with experimental data. The apparent relevance of the space-varying impedance hypothesis leads to the need for investigation of a TM cutoff and any resulting evanescent modes.

APPENDIX: OSSICULAR CHAIN MODEL

Following are details about each section, as required to implement the OC model.

1. Malleus and incus

Those two ports are in the form of Fig. 1, with

$$\text{Malleus: } Y = \frac{R_{im}C_{im}s}{1 + R_{im}C_{im}s} \quad \text{and} \quad Z = M_m,$$

$$\text{Incus: } Y = \frac{R_{is}C_{is}s}{1 + R_{is}C_{is}s} \quad \text{and} \quad Z = M_i.$$

The filters being of order greater than 1, final states of the filters need to be stored from one time step to the other to ensure proper signal processing. Note that this study has approximated the two ossicles characteristic impedance by $\sqrt{M/C}$, i.e., neglecting the joint resistance in the computation, which is a good approximation at low frequencies (in the long wavelength limit). From Campbell (1922), both two ports are low-pass filters having a cutoff frequency of $f_0 = 1/2\pi\sqrt{MC}$. For the chosen parameters of our simulations

$$\text{Malleus: } f_0 = 17.71 \text{ kHz},$$

$$\text{Incus: } f_0 = 238.3 \text{ kHz}.$$

We can then conclude that the incus does not have much influence over the propagating wave in the considered frequency range. However, the malleus filter has probably a slight influence over very high frequencies (over 15 kHz), which the authors have actually observed when playing with the parameters: increasing the malleus mass does lower the cutoff frequency and brings some perturbations to the input impedance at very high frequencies.

2. Middle-ear attic ligaments

For the attic ligaments we include the anterior malleal ligament, anchoring the manubrium and TM at the tympanic ring to the attic, and the posterior incudal ligament, anchoring the incus to the attic. These two ligaments are represented by a single compliance, in series with the malleus mass. The attic ligaments account for the residual stiffness for the short-circuit boundary condition corresponding to the disarticulated stapes experiment (Puria and Allen, 1998).

This two port is special because it does not have any explicit shunt admittance: consequently, the usual "ABCD matrix" method cannot be directly applied, because the method requires the estimate of the characteristic impedance for each section (i.e., Eq. (6)). The resolution of this has been the addition of a shunt (rotational) mass, making the first two port a high-pass filter (Campbell, 1922). Our reasoning as to why this element must be a mass is that every horn results from a spatially varying impedance having a cutoff, leading to a high-pass behavior, presumably with a low cutoff frequency (e.g., well below 1 kHz). This mass element could then be associated with the TM rather than the OC. This is an interesting problem, related to that described in Rosowski *et al.* (1988). Its value is equally difficult to estimate, thus it has been adjusted empirically: the authors have decided to simply decrease the cutoff frequency so that the mass does not disrupt the system response. The mass is then set to very high values, resulting in a cutoff frequency around 100 Hz. This ensures a proper reflection of low frequencies, without a noticeable attenuation above 1 kHz. This problem clearly requires an experimental investigation, well beyond the scope of the present modeling effort. The present implementation of this two port is to be seen as a stepping stone toward the resolution of the TM cutoff, rather than an actual solution.

3. Stapes and cochlear load

The cochlear impedance model is taken from Lynch *et al.* (1982), modeled by a cochlear resistor R_c, shunted by a series mass and resistor M_0 and R_0, representing the helicotrema. The round window is represented by a series compliance C_{rw}. The model published by Lynch *et al.* (1982) also includes another mass, in series with the shunt association which had little utility, and thus was dropped, as by Puria and Allen (1991). The final load is treated as a simple one port, since the wave transmitted into the cochlea is not developed in the present analysis. A single frequency-dependent reflection coefficient $\mathcal{R}_{\text{load}}(s)$ is derived from this load impedance:

$$Z_{\text{load}}(s) = M_s s + \frac{1}{C_{al}s} + R_{al} + \frac{R_c(M_0 s + R_0)}{R_c + M_0 s + R_0} + \frac{1}{C_{rw}s}, \tag{A1}$$

giving a cochlear reflectance of

$$\mathcal{R}_{\text{load}}(s) = \frac{Z_{\text{load}}(s) - z_{0_i}}{Z_{\text{load}}(s) + z_{0_i}}, \tag{A2}$$

where z_{0_i} is the incus characteristic impedance, $\sqrt{M_i/C_{is}}$; in fact, since the stapes is included in the final load impedance, the reflection coefficient must be computed using the incus impedance, not the stapes. The reflected sample is obtained by filtering the forward output of the incus two port. Note that the round window compliance is not expected to have much influence here since, according to both Puria and Allen (1998) and Lynch *et al.* (1982), its value is around 50 times lower than the annular ligament compliance. It is included in the model, however, because it is associated with an actual physical element of the ear and could have a more serious influence in further work on pathologic ears.

4. Sampling rate

With the lumped-parameter approach, delay is no longer simulated by shifting samples along the transmission line, but directly by filtering. It is then critical to set the filters parameters properly so that the phase shift of each two port is physically relevant. A critical factor is the sampling rate.

TABLE I. Model parameter values (1/2).

Parameter	Value
Sampling rate [Hz]	$f_s=1.96\times10^6$
Ear canal:	
Canal length [cm]	$L_{ec}=0.15$
Spatial period [cm]	$\Delta x_{ec}=0.018$
Speed of sound [cm/s]	$\mathcal{C}_{ec}=34{,}720$
Canal diameter [cm]	$D_{ec}=0.46$
Canal cross-section area [cm^2]	$A_{ec}=0.17$
Characteristic impedance [g/(cm^4 s)]	$Z^a_{ec}=245.0$
Tympanic membrane:	
TM diameter [cm]	$D_{tm}=0.72$
TM area [cm^2]	$A_{tm}=0.41$
Number of annuli	$N=71$
Ratio of speeds	$q=3.4$
Wave speed [cm/s]	$\mathcal{C}_{tm}=10{,}212$
Spatial period [cm]	$\Delta r_{tm}=0.005$
Angle with respect to canal axis [°]	$\alpha=40$
Impedance ratio	$\text{Ratio}_{\text{TM}}=7.5$
Impedance at TM output [g/(cm^4 s)]	$Z^a_{tm_{out}}=1837.3$
Ossicular chain:	
Middle ear cavity cross-section area [cm^2]	$A_{me}=A_{tm}=0.41$ (0.41)
Ossicular chain lever ratio	$N_{\ell r}=2$ (2)
Malleus ligaments resistance [dyne s/cm]	$R^m_m=60$ (30, 2)
Malleus ligaments compliance [cm/dyn]	$C^m_m=1.90\times10^{-6}$ $(8.89\times10^{-7}, 2.14)$
Malleus ligaments inertial mass [g]	$M^m_{mh}=1.39$
Malleus mass [g]	$M^m_m=0.0028$ (0.0028)
IM-joint resistance [dyne s/cm]	$R^m_{im}=7.50$ (7.50)
IM-joint compliance [cm/dyn]	$C^m_{im}=2.91\times10^{-8}$ $(2.87\times10^{-8}, 1.01)$
Malleus impedance [g/(cm^4 s)]	$Z^m_m=308.86$

TABLE II. Model parameter values (2/2).

Parameter	Value
Incus mass [g]	$M^m_i=8.25\times10^{-4}$ (8.25×10^{-4})
IS-joint resistance [dyne s/cm]	$R^m_{is}=37.5$ (75, 2)
IS-joint compliance [cm/dyn]	$C^m_{is}=5.41\times10^{-10}$ $(5.39\times10^{-10}, 1.00)$
Stapes mass [g/cm^4]	$M^a_s=24.75$ (24.75)
Annular ligament resistance [dyne s/cm^5]	$R^a_{al}=7.5\times10^5$(7.5$\times$ 10^5)
Annular ligament compliance [cm^5/dyn]	$C^a_{al}=3.81\times10^{-11}$ $(2.52\times10^{-11}, 1.51)$
Stapes footplate area[cm^2]	$A_{fp}=0.0126$ (0.0126)
Helicotrema mass [g/cm^4]	$M^a_0=3750$ (16875, 0.22)
Helicotrema resistance [dyne s/cm^5]	$R^a_0=7.5\times10^5$ (2.10$\times$ 10^6, 0.36)
Cochlea input impedance [dyne s/cm^5]	$R^a_c=9.0\times10^6$ (9.0$\times$ 10^6)
Round window compliance [cm^5/dyn]	$C^a_{rw}=1.33\times10^{-9}$ (1.33×10^{-9})

Typical delays in the ossicles are in the order of the microsecond (Puria and Allen, 1998): proper handling of such small delays requires high sampling rates, namely, in the order of 2 MHz (more precisely, $f_s=1.96$ MHz). Once derived, f_s is used to compute the spatial sampling on the TM and in the canal. This may be a detail where some future simplification might occur. For now we remain detailed, so that we can accurately simulate the fine structure of various pathologies, rather than be fast (a possible goal of such future models).

5. Choice of parameters

Model parameters are summarized in Tables I and II. Acoustical units are specified with superscript a, mechanical units with superscript m, following the representation used by Puria and Allen (1998). The various middle ear model parameters are inspired by the values from Puria and Allen (1998), and Lynch *et al.* (1982) for the cochlea model (i.e., M_0, R_0, R_c, and C_{rw}). Since these two studies do not take into account the TM impedance transformation ratio, Ratio_{TM}, their values have been scaled by this factor before being used in our model. Note that for the two joint compliances, C_{im} and C_{is}, the formula used in our work (Eq. (6)) differs slightly from the ones mentioned by Puria and Allen (1998, Eqs. 16 and 17), because we do not allow an IM joint slippage factor, and our IM joint is located on the left side of the OC transformer. Our approach, as in (Puria and Allen, 1998), is to start from the earlier values and then to adjust them to best match experimental impedance data of Allen (1986). The parameters were adjusted manually, and the influence of each one is intuitively understood. In Tables I and II, previously published (scaled) values are indicated in brackets, along with the relative variation we have applied to get the values that are actually used in the model (not indicated when values are equal). In most cases, this factor lies between 0.5 and 2, which shows that our model is consistent with the previous analysis. Only helicotrema parameters had to be decreased significantly to obtain a proper match, as discussed further.

It is interesting to question the difference between the malleus and incus mass. The values reported here are very close to the ones from Puria and Allen (1998). In their paper, they compare their malleus mass to experimental measurements by Lynch (1981); Lynch *et al.* (1994): their mass is smaller by a factor of around 4. According to them, "this factor might be accounted for by the smaller size of animals used in [their] study in comparison to those of Lynch *et al.* (1994). Another explanation might be the differences in the radius of gyration between Lynch's measurements and those in [their] study." However, the ratio of malleus mass to incus mass is consistent with the values from Lynch. No reference is made to the stiffness values. It is probably relevant to say that the incus is smaller than the malleus, hence the difference of mass.

Allen, J. B. (**1986**). "Measurement of eardrum acoustic impedance," in *Peripheral Auditory Mechanisms*, edited by J. B. Allen, J. L. Hall, A. Hubbard, S. T. Neely, and A. Tubis (Springer-Verlag, New York), pp. 44–51.

Allen, J. B. (**2001**). "Nonlinear cochlear signal processing," in *Physiology of the Ear*, 2nd ed. (Singular Thomson Learning, San Diego), Chap. 19, pp. 393–442.
Allen, J. B. (**2003**). "Amplitude compression in hearing aids," in *MIT Encyclopedia of Communication Disorders* (MIT Press, Boston), Chap. Part IV, pp. 413–423.
Allen, J. B., Jeng, P. S., and Levitt, H. (**2005**). "Evaluating human middle ear function via an acoustic power assessment," J. Rehabil. Res. Dev. **42**(4), 63–78.
Bekesy, G. v., and Rosenblith, W. A. (**1951**). "The mechanical properties of the ear," in *Handbook of Experimental Psychology*, edited by S. S. Stevens (Wiley, New York).
Beranek, L. L. (**1954**). *Acoustics* (McGraw-Hill, New York).
Bilbao, S. D. (2001). "Wave and scattering methods for the numerical integration of partial differential equations," Ph.D. thesis, Stanford University.
Brillouin, L. (**1953**). *Wave Propagation in Periodic Structure*, 2nd ed. (Dover, New York).
Campbell, G. A. (**1922**). "Physical theory of the electric wave-filter," Bell Syst. Tech. J. **1**(2), 1–32.
Fay, J. P. (2001). "Cat eardrum mechanics," Ph.D. thesis, Stanford University.
Fay, J. P., Puria, S., and Steele, C. R. (**2002**). "Cat eardrum response mechanics," *Presented at the Calladine Festschrift*, edited by S. Pellegrino (Kluwer, The Netherlands).
Fay, J. P., Puria, S., and Steele, C. R. (**2006**). "The discordant eardrum," Proc. Natl. Acad. Sci. U.S.A. **103**(52), 19743–19748.
Funnel, W. R. J., and Decraemer, W. F. (**1996**). "On the incorporation of moire shape measurements in finite element models of the cat eardrum," J. Acoust. Soc. Am. **100**(2), 925–932. Part 1.
Funnel, W. R. J., Decraemer, W. F., and Khanna, S. M. (**1987**). "On the damped frequency response of a finite-element model of the cat eardrum," J. Acoust. Soc. Am. **81**(6), 1851–1859.
Funnel, W. R. J., and Laszlo, C. A. (**1978**). "Modeling of the cat eardrum as a thin shell using the finite-element method," J. Acoust. Soc. Am. **63**, 1461–1466.
Goode, R. L., and Killion, M. C. (**1987**). "The middle ear from the standpoint of the surgeon and the acoustician," *Paper presented at the 113th meeting of the Acoustical Society of America*, Indianapolis, Indiana.
Guinan, Jr., J. J., and Peake, W. T. (**1967**). "Middle-ear characteristics of anesthetized cats," J. Acoust. Soc. Am. **41**(5), 1237–1261.
Kelly, J. L., and Lochbaum, C. C. (**1963**). "Speech synthesis," in *Proceedings of the Fourth International Congress on Acoustics* (ICA, Copenhagen), Chap. 42, pp. 1–4.
Kinsler, L. E., Frey, A. R., Coppens, A. B., and Sanders, J. V. (**2000**). *Fundamentals of Acoustics*, 4th ed. (Wiley, New York).
Leach, W. M. (**1996**). "A two-port analogous circuit and spice model for salmon's family of acoustic horns," J. Acoust. Soc. Am. **99**(3), 1459–1464.
Lim, D. J. (**1968a**). "Tympanic membrane electron microscopic observation part i: Pars tensa," Acta Oto-Laryngol. **66**, 181–198.
Lim, D. J. (**1968b**). "Tympanic membrane part ii: Pars flaccida," Acta Oto-Laryngol. **66**, 515–532.
Lynch, T. J., III. (1981). "Signal processing by the cat middle-ear: Admittance and transmission, measurements and model," Ph.D. thesis, Massachusetts Institute of Technology.
Lynch, T. J., III, Nedzelnitsky, V., and Peake, W. T. (**1982**). "Input impedance of the cochlea in cat," J. Acoust. Soc. Am. **72**(1), 108–130.
Lynch, T. J., III, Peake, W. T., and Rosowski, J. J. (**1994**). "Measurements of the acoustic input impedance of cat ears: 10 Hz to 20 kHz," J. Acoust. Soc. Am. **96**, 2184–2209.
Olson, E. S. (**1998**). "Observing middle ear and inner ear mechanics with novel intracochlear pressure sensors," J. Acoust. Soc. Am. **103**, 3445–3463.
Oppenheim, A. V., Schafer, R. W., and Buck, J. R. (**1999**). *Discrete-Time Signal Processing*, 2nd ed. (Prentice–Hall, Upper Saddle River, NJ).
Parent, P. (2005). "Wave model of the tympanic membrane," Master's thesis, University of Illinois at Urbana-Champaign.
Parent, P., and Allen, J. B. (**2006**). "Tympanic membrane model," Abstract presented at the *29th annual midwinter meeting of the Association for Research in Oto-laryngology*, Baltimore.
Puria, S. (**1991**). "A physical model for the middle ear cavity," J. Acoust. Soc. Am. **89** Suppl., 1864.
Puria, S. (**2003**). "Measurements of human middle ear forward and reverse acoustics: Implications for otoacoustics emissions," J. Acoust. Soc. Am. **113**(5), 2773–2789.
Puria, S., and Allen, J. B. (**1991**). "A parametric study of cochlear input impedance," J. Acoust. Soc. Am. **89**, 287–309.
Puria, S., and Allen, J. B. (**1998**). "Measurements and model of the cat middle ear: Evidence of tympanic membrane acoustic delay," J. Acoust. Soc. Am. **104**(6), 3463–3481.
Puria, S., and Fay, J. (**2001**). "Human eardrum and ossicles: Two-port matrix measurements," *Abstract presented at the Association for Research in Otolaryngology*.
Puria, S., and Rosowski, J. J. (**1996**). "Measurement of reverse transmission in the human middle ear: Preliminary results," in *Diversity in Auditory Mechanics*, edited by E. R. Lewis, G. R. Long, R. F. Lyon, P. M. Narins, C. R. Steele, and E. L. Hecht-Poinar (World Scientific, Singapore).
Rabbitt, R. D., and Holmes, M. H. (**1986**). "A fibrous dynamic continuum model of the tympanic membrane," J. Acoust. Soc. Am. **80**(6), 1716–1728.
Rabbitt, R. D., and Holmes, M. H. (**1988**). "Three-dimensional acoustic waves in the ear canal and their interaction with the tympanic membrane," J. Acoust. Soc. Am. **83**, 1064–1080.
Rosowski, J. J., Carney, L. H., and Peake, W. T. (**1988**). "The radiation impedance of the external ear of cat: Measurements and applications," J. Acoust. Soc. Am. **84**(5), 1695–1708.
Rosowski, J. J., Cosme, F., Ravicz, M. E., and Rodgers, M. T. (**2006**). "Real-time opto-electronic holographic measurements of the sound-induced displacements of tympanic membranes," Paper presented at the *29th annual midwinter meeting of the Association for Research in Otolaryngology*, Baltimore.
Rosowski, J. J., Davis, P. J., Merchant, S. N., Donahue, K. M., and Coltrara, M. D. (**1990**). "Cadaver middle ears as models for living ears: Comparisons of middle-ear input immittance," Ann. Otol. Rhinol. Laryngol. , 403–412.
Salmon, V. (**1946a**). "Generalized plane wave horn theory," J. Acoust. Soc. Am. **17**(3), 199–211.
Salmon, V. (**1946b**). "A new family of horns," J. Acoust. Soc. Am. **17**(3), 212–218.
Sen, D., and Allen, J. B. (**2006**). "Functionality of cochlear micromechanics – as elucidated by the upward spread of masking and two tone suppression," Acoust. Aust. **34**(1), 43–51.
Shaw, E. A. G. (**1977**). "Eardrum representation in middle-ear acoustical networks," J. Acoust. Soc. Am. **62** Suppl. 1, S102.
Shaw, E. A. G., and Stinson, M. R. (**1981**). "Network concepts and energy flow in the human middle ear," J. Acoust. Soc. Am. **69**(S44), S43.
Stinson, M. R. (**1990**). "Revision of estimates of acoustic energy reflectance at the human eardrum," J. Acoust. Soc. Am. **88**(4), 1773–1778.
Stinson, M. R., and Daigle, G. A. (**2005**). "Comparison of an analytic horn equation approach and a boundary element method for the calculation of sound fields in the human ear canal," J. Acoust. Soc. Am. **118**(4), 2405–2411.
Stinson, M. R., and Khanna, S. M. (**1989**). "Sound propagation in the ear canal and coupling to the eardrum, with measurements on model systems," J. Acoust. Soc. Am. **85**(6), 2481–2491.
Stinson, M. R., and Khanna, S. M. (**1994**). "Spatial distribution of sound pressure and energy flow in the ear canals of cats," J. Acoust. Soc. Am. **96**(1), 170–180.
Stinson, M. R., Shaw, E., and Lawton, B. (**1982**). "Estimation of acoustical energy reflectance at the eardrum from measurements of pressure distribution in the human ear canal," J. Acoust. Soc. Am. **72**, 766–773.
Wegel, R. L., and Lane, C. E. (**1924**). "The auditory masking of one pure tone by another and its probable relation to the dynamics of the inner ear," Phys. Rev. **23**, 266–285.
Zwislocki, J. (**1957**). "Some impedance measurements on normal and pathological ears," J. Acoust. Soc. Am. **29**(12), 1312–1317.
Zwislocki, J. (**1962**). "Analysis of the middle-ear function. Part I: Input impedance," J. Acoust. Soc. Am. **34**(8, Part 2), 1514–1523.